Integrated ternary bionanocomposites with superior mechanical performance via the synergistic role of graphene and plasma treated carbon nanotubes.

Roberto Scaffaro*, Andrea Maio

Department of Engineering, University of Palermo, Viale delle Scienze, Ed. 6, 90128, Palermo (Italy)

*corresponding author: roberto.scaffaro@unipa.it

Abstract

Herein, we prepared an integrated ternary bionanocomposite based on polylactic acid (PLA) as a host polymer and two different forms of carbon fillers, i.e. graphene nanoplatelets (GNPs) and carbon nanotubes (CNTs), used simultaneously at extremely low concentrations, relying on the synergistic effect of CNT and graphene nanoreinforcement and a novel, multi-step procedure to achieve a high level dispersion. The results indicated that this multi-step approach allows stiffness increments up to +66%, with simultaneous enhancement of tensile strength (up to +44%), and elongation at break (up to +36%) with respect to neat PLA, by adding an extremely low content (0.5 wt.%) of a hybrid combination of CNTs and GNPs. The development of a multistep strategy to achieve molecular level dispersion of multifunctional nanoparticles integrated in a fully renewable polymer matrix allows the premise of industrial-scale production of advanced bionanocomposites with outstanding properties at extremely low loadings.

Keywords: Graphene; CNT; nanocomposites; mechanical properties.

1. Introduction

The growing interest towards carbon-based nanomaterials, including carbon nanotubes (CNTs) and graphene, mainly relates to their intriguing properties as conductive fillers for the fabrication of electric/electronic devices, which production volumes dramatically raised in the last recent years [1–7]. On the other hand, the increasing concern for environmental issues responds to the need of developing eco-sustainable strategies, thus posing some limitations about processing protocols and materials adopted for the design of the items/devices capable to fulfill different demands [8,9]. One successful strategy can be the incorporation of conductive fillers within a renewable polymer matrix to create eco-friendly multifunctional materials [4,10]. Among biopolymers, polylactic acid (PLA) is one of the most widespread, owing to its unique combination of good mechanical performance and environmental stability with the possibility to be disintegrated under specific conditions, with demonstrated

biocompatibility [11,12]. These latter aspects enable its use for the realization of biomedical devices [13–15]. Several studies focused on the realization of PLA-based materials containing either CNTs or graphene derivatives, while only more recently, using a combination of the two fillers is gaining a significant interest [10,16–28] Previous works highlighted that the synergistic role of these two nanoparticles lies in their different interaction with cracks at different stages of fracture, since graphene causes localized mirocracking and crack deviation at the early stages of fracture, while CNTs ensure the debonding and fiber bridging mechanisms [29]. The main challenge, however, lies in achieving uniform and excellent dispersion and matrix-filler interfacial adhesion without adopting long-time consuming nor expensive protocols [30]. Liquid phase exfoliation of GNP into few-layered graphene can be easily achieved by using appropriate solvents, capable to interact with sp^2 domains, such as toluene, N-methyl-pyrrolidone (NMP), dimethylformamide (DMF), or dimethyl sulfoxide (DMSO) [31]. However, this technique presents some crucial drawbacks, associated to the limited amounts of graphene that can be obtained, as well as to the difficulties in solvent removal and for the natural re-stacking of graphene sheets occurring after solvent evaporation. In order to overcome these issues, we developed a multistep strategy ensuring both solvent evaporation and excellent dispersion of GNPs throughout the polymer together with the exfoliation of nanoplatelets into mono- or few-layers graphene sheets.

2. Materials and methods

2.1 Materials

The polymer matrix used in the frame of this work is a sample of a biodegradable PLA 4032D, supplied by Natureworks (USA), characterized by a low molar content of D-isomer (about 1.5%). It has a specific gravity of 1.24 g cm^{-1}, M_n=90000 Da, M_w=180000 Da.

Graphene nanoplatelets (GNPs), trade name xGnP®, Grade C, were supplied by XG Sciences Inc., Lansing, MI, USA. Each particle consists of several sheets of graphene with an average thickness of approximately 2-5 nm, average diameter between 1 and 2 μm, and a specific surface area of about 750 m^2/g [16,32,33].

2.2 Synthesis and functionalization of CNTs

A pictorial representation of synthesis and functionalization of CNTs, according to our previous works, is provided in **Fig. 1A**[1,2]**.** Briefly, CNTs were synthesized by fluidized bed chemical vapor deposition in a quartz reactor, involving a γ-alumina substrate impregnated with a catalyst (iron) as bed material. The iron content was 20 wt%. Ethylene was used as carbon source and nitrogen as fluidizing agent. The CNTs

production yield of the process was 500 $g \cdot h^{-1}$ and the catalyst showed a nanotubes selectivity close to 100%, as no amorphous carbon was found in the final product.

The purification process consists in three steps: (i) acid treatment, (ii) washing, and (iii) drying, carried out in the same device: a three-phase slurry bubble column, which bed motion is ensured by a nitrogen stream. CNTs batch size 50–300 g can be treated by this equipment, i.e. a quantity one order of magnitude higher than those reported in the scientific literature [34,35]. High values of final purity and reproducible results were achieved in relatively short times (150 min) and at relatively low temperatures (120–130 °C) by using 70 wt% H_2SO_4 solution. Evaporative crystallization of waste waters allows recovering aluminum and iron sulfates to be recycled for catalyst preparation. CNTs, having a purity degree of 99.1% and a l/d ratio equal to 900, underwent a surface oxidation by oxygen-plasma treatment [1,2]. The plasma reactor used for the surface treatment is a Tucano Gambetti apparatus, equipped with a high vacuum-pump (Pfeiffer). The cylindrical chamber (diameter=150mm, length=330 mm) has a volume of approximately 5.5 dm^3. The dark shield electrode and the power supply (RF=13.56MHz, 200W) are placed on top of the chamber. The flow of the air takes place automatically at vacuum level and power programmed in the recipes with two mass flow-controllers, and it is controlled by a microcomputer. In this case, air flow was set to 10 sccm, the vacuum level was $2 \cdot 10^{-4}$ bar and the vacuum was stabilized for 5 s prior to the process gas inlet. After gas inlet, the pressure in the chamber achieved a value of about 0.5 mbar and the treatment has been then carried out at 120 W for 6 min. The parameters were adjusted in order to minimize reverse bias. Further details about the choice of these parameters can be found in our previous works [1,2,36,37].

2.3 Preparation of PLA-GNP masterbatch (PGM)

The schematics of the preparation of PLA-GNP masterbatch (PGM) is depicted in **Fig. 1B**. GNP (700 mg) underwent chemical exfoliation via sonication in toluene (700 mL) for 4 hours, thereafter the graphene dispersion was added to a solution containing 6.3 g of PLA dissolved in 200 mL of dichloromethane/chloroform (90:10), sonicated and then transferred to a rotavapor. This simple strategy ensures yields of 100% and the total removal of solvents. High-speed rotation allows achieving exfoliated graphene into mono- or few-layers surrounded by PLA macromolecules. 7 grams of PLA-graphene masterbatch (PGM) product (containing 10% of graphene) can be collected in less than 30 minutes and then added (in different proportions) to further fresh polymer and plasma functionalized CNTs for achieving high performance bionanocomposites by simply melt processing at relatively low rotor speed (i.e. 64 rpm), thus minimizing the risk of PLA thermo-mechanical degradation. The main goal of this

approach lies in the possibility to rapidly obtain an amount of masterbatch sufficient to prepare different formulations of high-performance nanocomposites with extremely low filler contents.

2.4 Preparation of nanocomposites

The schematics of the preparative is provided in **Fig. 1C**. Nanocomposites containing O-CNTs and GNP were prepared according to two different techniques, namely direct melt mixing (method A) and melt intercalation of PGM, i.e. multi-step processing (method B).

In the case of A-series samples, PLA, O-CNTs and GNPs were mixed at the solid state and fed to a Brabender internal mixer in the desired proportions until a constant value of torque was achieved (usually within 6 minutes). In the case of B-series materials, PGM was added to PLA and O-CNTs in order to achieve the same formulations of A-series materials. Formulations and operating conditions adopted are listed in **Tab. 1**. Note that GNP were used together with CNTs in different mutual proportions, by keeping constant the total loading (i.e. 0.5 wt.%).

Tab. 1. Formulation of bionanocomposites

Sample code	Preparation technique	PLA (wt/wt%)	GNPs (wt/wt%)	O-CNTs (wt/wt%)	T (°C)	Rotor (rpm)	T (min)
C50/G0-A	Melt mixing	99.5	0	0.5	190	64	6
C35/G15-A	Melt mixing	99.5	0.15	0.35	190	64	6
C25/G25-A	Melt mixing	99.5	0.25	0.25	190	64	6
C15/G35-A	Melt mixing	99.5	0.35	0.15	190	64	6
C0/G50-A	Melt mixing	99.5	0.5	0	190	64	6
C35/G15-B	Multi-step	99.5	0.15	0.35	190	64	6
C25/G25-B	Multi-step	99.5	0.25	0.25	190	64	6
C15/G35-B	Multi-step	99.5	0.35	0.15	190	64	6
C0/G50-B	Multi-step	99.5	0.5	0	190	64	6

For each batch, the material collected after melt compounding was rapidly cooled in liquid nitrogen, ground into pellets and then processed into sheets by compression-molding by using a laboratory press (Carver, Wabash, IN, USA) at 190 °C and 100 bar for about 2 min. Finally, they were cut into specimens of appropriate geometry for further characterizations.

2.5 Characterizations

The morphology of nanohybrids was observed by scanning electron microscopy (SEM), carried out in an ESEM FEI QUANTA 200 microscope on both nanoparticles and nanostructured films. In this latter case, the samples were attached on an aluminum stub using an adhesive carbon tape and then sputter coated with gold (Sputtering Scancoat Six, Edwards) for 90 s under argon atmosphere, before imaging, in order to avoid electrostatic discharge during the tests. TEM measurements were performed by using a JEOL 2100 operating at 200 kV.

AFM measurements were performed by a Multimode V (Veeco Metrology) scanning probe microscope, equipped with a piezoscanner, at room temperature and under nitrogen atmosphere. More details can be found elsewhere [38,39]

X-ray photoelectron spectroscopy (XPS) measurements were collected by using an ESCALAB MkII (VG Scientific) spectrometer, equipped with a standard Al Kα excitation source and a 5-channeltron detection system for spectroscopic analysis. The pass energy was kept constant at 20 eV, and the analyzed area of the sample was about 5 mm in diameter. Spectroscopic data have been processed by Avantage v.5 software [40].

X-ray diffraction (XRD) analysis was performed by using an Empyrean PANalytical II diffractometer with a Cu Kα radiation source (λ = 1.5406 Å). This analysis was performed to investigate the structure of GNP and platelet thickness, *t*, (i.e. the stacked graphene layers into each platelet), which was calculated according to Scherrer's equation, as follows:

$$t = \frac{0.9\,\lambda}{\beta \cos\theta} \qquad (1)$$

where λ is the wavelength of the X-rays, β is the full width at half maximum (FWHM) of intensity band centered to 2θ maximum [23]. The interlayer distance ($d_{spacing}$) of GNP was calculated by Bragg's law:

$$d_{spacing} = \frac{n\,\lambda}{2\sin\theta} \qquad (2)$$

With n being an integer equal to 1 [23].

Tensile mechanical measurements were carried out by using a dynamometer (Instron model 3365, High Wycombe, UK) on rectangular shaped specimens (10×90 mm) cut off from films prepared by compression-molding as described above. Grip distance and crosshead speed were respectively set to 30 mm and 1 mm·min^{-1}.

3. Results and discussion

Figs. 2A-C provide the salient geometrical features of plasma treated CNTs (O-CNTs), whose diameter is ~10 nm and the mean length, accurately studied in our previous works, is equal to 1-2 μm. The effect of

plasma treatment on CNTs was evaluated by XPS provided in **Fig. 2D**. We chose to perform plasma treatment at low power and time aiming to impart a mild functionalization on defects and amorphous regions of CNTs while preserving their sp^2 domains [1,2]. This feature is particularly relevant, since allows maximizing CNTs dispersion within the host polymer for enhancing mechanical properties without affecting electrical performance. The intercalation of PLA macromolecules between graphene sheets in PGM was assessed by TEM and XRD and shown in **Fig. 3 A-C**. Pristine GNPs, Fig. 3A, are organized in micrometric or sub-micrometric aggregates but a closer inspection of surface reveals the presence of typical sp^2 pattern of graphenic materials (see inset of Fig. 3 A). By contrast, PGM shows exfoliated graphene under the form of mono- or few-layered lamellae, as visible in **Fig. 3 B**. In order to get some information about thickness and lateral size of GNP, AFM analysis was performed on GNPs after sonication in toluene and provided in **Figs 3 C-D**. Each nanoplatelet has a thickness equal to about 1-2 nm and a lateral size ranging around 1-2 μm.

XRD results of GNPs and PGM are provided in **Fig. 3E**. As regards GNP, it was found a peak at $2\theta=26°$ related to (002) plane of stacked lamellae [41–43]. No graphitic peak was detected in PGM, except for a broad band centered at $2\theta=16°$, due to a small amount of γ-form crystallites in PLA, which however is practically amorphous [44].

In a multiphasic system, beyond the nature of its components, morphology plays a key-role on the ultimate properties. Therefore, morphology of the samples prepared was studied by SEM. **Fig. 4** shows a survey view of the morphology of cryofractured cross-sections for all the systems investigated, useful to assess filler dispersion. More in detail, the morphology of A-series samples are provided in top panels (Figs 4A-E), whereas those of B-series samples were reported in bottom panels (Figs 4 F-J), together with that of PGM as control. Nanocarbons can be easily identified as bright dots (see C50/G0-A in panel A and PGM, Fig. 4F, which is mainly constituted by GNPs). By examining A-series samples it can be seen that direct melt mixing is able to disperse CNTs (Fig. 4A) but it does not lead to the disruption of GNPs aggregates either in ternary (Figs. 4 B-D) or binary samples (Fig. 4E). Furthermore, lack of adhesion and voids are visible in such structures even at low magnification. As regards B-series samples, reported in Figs 4 F-J, it can be observed a good dispersion with the absence of micrometric clusters/aggregates. Detailed micrographs of the nanocomposites surface morphology are provided in **Fig. 5** for evaluating the interfacial adhesion between the matrix and the two fillers. C50/G0-A, Fig. 5A, shows CNTs totally embedded into the matrix, owing to plasma-treatment. In fact, as already reported, this treatment induces oxygen-bearing moieties onto the sidewalls of nanotubes and enhance surface roughness via the introduction of defects in the graphenic lattice [1–4]. C0/G50-A, Fig. 5B, shows a poor adhesion between

GNP particles and PLA, whereas C0/G50-B, Fig. 5C, displays a high level of wettability, with GNP lamellae totally surrounded by the polymer. This different behaviour could be explained by considering that sonication and solvent treatment, while inducing GNPs exfoliation, likely increase the surface roughness of nanoparticles, thus promoting wettability. As a consequence of the different wettability of untreated and exfoliated GNPs, A-series materials (Figs D-F) all displayed voids symptomatic of scarce filler-matrix adhesion. It can be also highlighted that number of voids proved to increase with GNP content. The detailed micrographs showing cross-sections of B-series ternary nanocomposites, Figs G-I, display PLA-wrapped CNTs and GNP lamellae, symptomatic of a quite strong adhesion, apart from CNT/GNP ratio.

The salient properties derived from tensile tests, i.e. elastic modulus (E), tensile strength (TS), elongation at break (EB), are plotted as a function of CNT and GNP concentration and provided in **Figs 6 A-C**, respectively. **Fig. 6A** reports E plotted as a function of formulation, with this latter being expressed both as CNTs concentration (reported in blue) and GNPs content (in black), being the sum of GNP wt.% and CNT wt.% equal to 0.5 wt.%, for each sample. As regards the samples prepared by direct melt mixing (A-series materials), incorporating 0.5 wt.% CNTs led to a tensile modulus equal to 2.17 GPa, i.e. +45% when compared to that (1.5 GPa) of neat PLA. At the same loading level, GNPs seem to be unable to affect this property, which was found to remain much similar (~1.6 GPa) to that of neat PLA (1.5 GPa). Stiffness of materials containing a combination of CNT and GNP proved to be intermediate between those achieved with CNT only and GNP only, ranging from 1.55 GPa to 1.73 GPa. The samples prepared according to Method B showed a different trend since, in this latter case, exfoliated GNPs determined a strong increase of elastic modulus in C0/G50-B (2.3 GPa) and the hybrid bi-fillers led to mechanical properties higher than those of the samples containing single nanofillers, with tensile moduli equal to 2.35 GPa, 2.4 GPa and 2.5 GPa for C35/G15-B, C25/G25-B and C15/G35-B, respectively.

In order to interpret these results, Halpin-Tsai model was used to fit experimental data collected for the systems containing CNT only and GNP only, and provided in the same figure (see solid line labeled as E_{HT}) [45–47].

According to this model, in the case of a nanocomposite containing randomly oriented CNT, the tensile modulus E_C is determined by the following equation:

$$E_C = \frac{3}{8}E_L + \frac{5}{8}E_T \quad (3)$$

Where E_L and E_T are respectively the longitudinal and transverse moduli of the composite.

In this case, E_L and E_T are given by:

$$E_L = E_m\left[\frac{1+\xi\eta_L\upsilon_f}{1-\eta_L\upsilon_f}\right] \quad (4) \qquad E_T = E_m\left[\frac{1+2\eta_T\upsilon_f}{1-\eta_L\upsilon_f}\right] \quad (5)$$

Where υ_f and υ_m are the volume fractions of filler and PLA, η_L and η_T are constants given by:

$$\eta_L = \frac{\left(E_f/E_m\right)-1}{\left(E_f/E_m\right)+\xi} \quad (6) \qquad \eta_T = \frac{\left(E_f/E_m\right)-1}{\left(E_f/E_m\right)+2} \quad (7)$$

With E_f and E_m being respectively the Young's moduli of filler and PLA, while ξ, taking into account the filler aspect ratio, for 1D fillers is equal to:

$$\xi_{CNT} = \frac{2l}{d} \quad (8)$$

while *l* and *d* indicate respectively length and diameter of CNTs [27,28].

In the case of nanocomposites containing randomly dispersed GNP, instead, the equation for determining E_C is slightly different, as follows [17]:

$$E_C = 0.49\ E_L + 0.51\ E_T \quad (9)$$

Eqs (4-7) are still applicable but in this case:

$$\xi_{GNP} = \frac{2w}{3t} \quad (10)$$

With *w* and *t* being respectively the lateral size (under the assumption of with=length) and thickness of nanoparticles [17].

Volume fractions are determined from the weight fractions and the densities of each component. GNP density was considered being equal to 2.2 g/cm^3, as declared by producer, whereas that of CNTs, which can be regarded as hollow cylinders, was approximated according to eq. (11):

$$\rho_{CNT} = \rho_G\frac{d^2-d_i^2}{d^2} \quad (11)$$

Where ρ_G is the graphite density, while *d* and d_i are outside and inside diameters of CNTs, respectively. Under these hypotheses, ρ_{CNT}~ 1.95 g/cm^3, consistently with other reports [48,49].

Em, experimentally measured by tensile tests on neat PLA, was found to be equal to 1.5 GPa, whereas for E_f values, 0.9 TPa for CNTs and 1 TPa for GNP were taken from the scientific literature [50]. Hence, a crucial factor that can affect the stiffness in a nanocomposite is the filler aspect ratio. It should be noted that aspect ratio of CNTs is around 900-1000, whereas for GNPs it may vary up to almost 1000,

depending on the extent of aggregation, exfoliation, and so on. In fact, GNP are constituted by submicrometric aggregates of platelets having a lateral size of 2-5 μm and a thickness equal to 2-5 nm, according to the results of morphological analyses and Scherrer equation. Based on this consideration, using Method B ensures obvious advantages, since the possibility to disperse and exfoliate the aggregates of GNP into few- or monolayer sheets leads to a more extended interphase. Indeed, it should be considered that GNP is a pseudo-2D filler, constituted by few-layer graphene sheets aggregated into 3D clusters. Direct melt mixing was found to be not appropriate for disrupting the aggregates, whereas the two-step method, with the aid of ultrasonication and solvents, proved to be able to pre-disperse and/or even to exfoliate the nanoplatelets into mono- or few-layer graphene sheets. This latter feature dramatically increases the overall interphase volume and the aspect ratio of the nanoparticles, with positive repercussions on the mechanical performance of the resulting nanocomposites. Therefore, differently from A-series materials, where no synergetic effect was detected, PLA/GNP/CNT systems prepared by method B showed mechanical performance higher than those of PLA/GNP and PLA/CNT, likely due to the formation of a 3D interconnected framework, which somehow increases the dispersability of the two components throughout the matrix [24]. However, it should be noted that B-series materials display E values lower than those predicted by Halpin-Tsai (see E_{HT} line in the graph of Fig. 6A). As regards tensile strength, **Fig. 6B**, it can be noted that nanocomposites generally displayed TS values ranging from 50 MPa to 75 MPa, depending on formulation, i.e. generally higher than that of neat PLA (52 MPa), except for C0/G50-A. Two different trends with the formulation were found depending on the preparation method. For A-series materials, the highest TS value was displayed by C50/G0-A (60 MPa), whereas C0/G50-A showed the lowest value of this property (50 MPa). Ternary materials exhibited intermediate TS values, with TS practically showing a monotonic, decreasing trend with GNP content. B-series materials, instead, followed a different trend. First, for binary nanocomposites, it was observed that C0/G50-B shows a TS value (70 MPa) higher than C50/G0-A. Moreover, some ternary materials, i.e. C25/G25-B (TS=73 MPa) and C15/G35-B (TS=75 MPa), displayed values of TS higher than those shown by binary nanocomposites. Among the parameters influencing TS in a nanocomposite, the interfacial adhesion between its components plays a key-role [51,52]. It was highlighted that method B enhances the mutual affinity between PLA and GNP (see again Figs. 4-5), whereas method A caused lack of adhesion. It should be noted that, however, the presence of hybrid filler brings some benefits even in A-series materials at low GNP content.

Elongation at break (EB), **Fig. 6C**, was found to be almost unaffected by the presence of GNP, while a slight reduction of stretchability was detected in the case of CNTs. Interestingly, although moderate EB values were detected in all of the materials, it was generally found that nanocomposites display a relatively higher stretchability than neat PLA, except for C50/G0-A. This feature could be due to the relatively low amount of filler and/or to the small fillers size. Notably, B-series samples displayed the highest values of this property.

The synergetic effect of CNT and graphene (or GNP) on the properties of PLA-based nanocomposites can be conveniently elucidated by using equation (1) [53]:

$$\text{Synergistic efficiency} = [2P_{hyb} - (P_{CNT} + P_G)]/(P_{CNT} + P_G)] \quad (12)$$

where P_{CNT}, P_G and P_{hyb} represent the generic property measured for PLA loaded with CNTs, graphene and a hybrid combination of graphene and CNTs, respectively.

This parameter is of great importance for investigating the eventual changes of the tailored properties upon changing the graphene to CNTs ratio, thus optimizing processing and formulation for the achievement of certain targets. The synergistic effect of the two fillers on stiffening, strengthening and stretchability of PLA is provided in **Figs 6D-F**, respectively. Of course, in the case of synergy, the synergistic efficiency has positive values (see green-filled area in the plots), whereas it assumes negative values in the case of destructive interference (red-filled area). Of course, this parameter is equal to zero in the absence of interactions. As one can see, the simultaneous use of CNT and GNP determines a synergistic efficiency in stiffness (Fig. 6D) only when B method is adopted. In fact, due to the aforementioned dispersion issues, method A is likely inadequate to disrupt GNP aggregates, thus leading to a decrease of filler aspect ratio and interphase volume. Hybrid loading of GNP and CNT leads to a synergy in strengthening effect (Fig. 6E) apart from the preparation technique, although B-materials display a higher synergetic effect of bi-filler combination. As regards stretchability, Fig. 6F, B-materials led to synergy efficiency ranging from 15% to 20%, depending on formulation, whereas A-method results in destructive interference or no synergy. It can be noted that the highest synergetic effects were recognized in C15/G35-B for all of the properties tested. **Fig. 7** reports further details of the cross-sections of C0/G50-A (A), C0/G50-B (B), C50/G0-A (C), C35/G15-B (D), C25/G25-B (E) and C15/G35-B (F) after tensile tests, useful to describe interphase features of such samples and to explain the high synergetic effects detected in B-series samples. The influence of preparation method on the PLA-GNP adhesion can be assessed by observing SEM micrographs of C0/G50-A (panel A), C0/G50-B (panel

B). C0/G50-A exhibits micrometric GNP clusters, poorly adhered to PLA. By contrast, C0/G50-B shows few-layered GNP lamellae strongly bonded to the matrix. Fig. 7C demonstrates that, differently from GNPs, O-CNTs exhibit a strong adhesion to PLA when directly melt mixed. B-series ternary samples display a rough surface, symptomatic of a good stress transfer and no pull-out was detected. Furthermore, those containing a higher content of CNTs (C35/G15-B, Fig. 7D, and C25/G25-B, Fig. 7E) displayed bridging phenomena. Examining the cross-section after tensile failure of C15/G35-B, Fig. 7F, which showed the best mechanical performance, it was possible to detect a 3D hybrid network totally surrounded by PLA.

4. Conclusion

Ternary nanohybrids based on PLA, CNTs and graphene (either in its exfoliated form or stacked into nanoplatelets) were succesfully prepared, aiming at gathering some green and biological features of PLA with the unique electrical and mechanical properties of the nanofillers into a multifunctional device. A novel, multi-step fabrication procedure was implemented to achieve a molecular-level dispersion, thus relying on the synergistic effect of the two fillers on some ultimate properties. The synergy efficiency of bi-filler loading on stiffness, strengthening and toughening of the ternary materials was measured and correlated to preparative method and formulation, as well as to the structural features of resulting materials. With respect to direct melt mixing, the multi-step preparative gave rise to materials displaying higher mechanical performance, presumably due to a more uniform dispersion/exfoliation of nanofillers, with a consequent increase of GNP aspect ratio that determined an increased volume of interphase. Based on similar considerations, the hybrid network constituted by 1D and 2D fillers results in stiffening and strengthening effects higher than those achieved by using CNTs only or graphene only. In conclusion, biocompatible, renewable, eco-friendly materials providing exceptional mechanical, thermal, and electrical properties were successfully fabricated by a novel multi-step procedure. The excellent performance observed with adding only 0.5 wt% of bi-filler enables the possibility to provide PLA with some additional properties of enormous interest without compromising other peculiar features of the polymer, such as biodegradability, biocompatibility, renewability and density.

References

[1] Scaffaro R, Maio A, Tito AC. High performance PA6/CNTs nanohybrid fibers prepared in the melt. Compos Sci Technol 2012;72:1918–23. doi:10.1016/j.compscitech.2012.08.010.

[2] Maio A, Botta L, Tito AC, Pellegrino L, Daghetta M, Scaffaro R. Statistical Study of the Influence of CNTs Purification and Plasma Functionalization on the Properties of Polycarbonate-CNTs Nanocomposites. Plasma Process Polym 2014;11:664–77. doi:10.1002/ppap.201400008.

[3] Oh JY, Jun GH, Jin S, Ryu HJ, Hong SH. Enhanced Electrical Networks of Stretchable Conductors with Small Fraction of Carbon Nanotube/Graphene Hybrid Fillers. ACS Appl Mater

Interfaces 2016;8:3319–25. doi:10.1021/acsami.5b11205.

[4] Paszkiewicz S, Szymczyk A, Sui XM, Wagner HD, Linares A, Ezquerra TA, et al. Synergetic effect of single-walled carbon nanotubes (SWCNT) and graphene nanoplatelets (GNP) in electrically conductive PTT-block-PTMO hybrid nanocomposites prepared by in situ polymerization. Compos Sci Technol 2015;118:72–7. doi:10.1016/j.compscitech.2015.08.011.

[5] Ferreira F V, Brito FS, Franceschi W, Simonetti EAN, Cividanes LS, Chipara M, et al. Functionalized graphene oxide as reinforcement in epoxy based nanocomposites. Surfaces and Interfaces 2018;10:100–9. doi:10.1016/j.surfin.2017.12.004.

[6] Ferreira F V, Francisco W, Menezes BRC, Brito FS, Coutinho AS, Cividanes LS, et al. Correlation of surface treatment, dispersion and mechanical properties of HDPE/CNT nanocomposites. Appl Surf Sci 2016;389:921–9. doi:https://doi.org/10.1016/j.apsusc.2016.07.164.

[7] Ferreira F V, Menezes BRC, Franceschi W, Ferreira E V, Lozano K, Cividanes LS, et al. Influence of carbon nanotube concentration and sonication temperature on mechanical properties of HDPE/CNT nanocomposites. Fullerenes, Nanotub Carbon Nanostructures 2017;25:531–9. doi:10.1080/1536383X.2017.1359553.

[8] Morreale M, Scaffaro R, Maio A, Mantia FP La. Effect of adding wood flour to the physical properties of a biodegradable polymer. Compos Part A Appl Sci Manuf 2008;39:503–13. doi:http://dx.doi.org/10.1016/j.compositesa.2007.12.002.

[9] Spinella S, Lo Re G, Liu B, Dorgan J, Habibi Y, Leclére P, et al. Polylactide/cellulose nanocrystal nanocomposites: Efficient routes for nanofiber modification and effects of nanofiber chemistry on PLA reinforcement. Polym (United Kingdom) 2015;65:9–17. doi:10.1016/j.polymer.2015.02.048.

[10] Correia Pinto V, Ramos T, Alves S, Xavier J, Tavares P, Moreira P, et al. Dispersion and failure analysis of PLA, PLA/GNP and PLA/CNT-COOH biodegradable nanocomposites by SEM and DIC inspection. Eng Fail Anal 2016. doi:10.1016/j.engfailanal.2016.06.009.

[11] Fukushima K, Feijoo JL, Yang M-C. Comparison of abiotic and biotic degradation of PDLLA, PCL and partially miscible PDLLA/PCL blend. Eur Polym J 2013;49:706–17. doi:https://doi.org/10.1016/j.eurpolymj.2012.12.011.

[12] Scaffaro R, Botta L, Lopresti F, Maio A, Sutera F. Polysaccharide nanocrystals as fillers for PLA based nanocomposites. Cellulose 2017;24:447–78. doi:10.1007/s10570-016-1143-3.

[13] Scaffaro R, Lopresti F, Botta L, Rigogliuso S, Ghersi G. Preparation of three-layered porous PLA/PEG scaffold : relationship between morphology , mechanical behavior and cell permeability. J Mech Behav Biomed Mater 2016;54:8–20. doi:10.1016/j.jmbbm.2015.08.033.

[14] Blaker JJ, Lee K-Y, Mantalaris A, Bismarck A. Ice-microsphere templating to produce highly porous nanocomposite PLA matrix scaffolds with pores selectively lined by bacterial cellulose nano-whiskers. Compos Sci Technol 2010;70:1879–88. doi:10.1016/j.compscitech.2010.05.028.

[15] Zhou C, Shi Q, Guo W, Terrell L, Qureshi AT, Hayes DJ, et al. Electrospun bio-nanocomposite scaffolds for bone tissue engineering by cellulose nanocrystals reinforcing maleic anhydride grafted PLA. ACS Appl Mater Interfaces 2013;5:3847–54. doi:10.1021/am4005072.

[16] Scaffaro R, Botta L, Maio A, Mistretta MC, La Mantia FP. Effect of Graphene Nanoplatelets on the Physical and Antimicrobial Properties of Biopolymer-Based Nanocomposites. Materials (Basel) 2016;9:351. doi:10.3390/ma9050351.

[17] Gao Y, Picot OT, Bilotti E, Peijs T. Influence of filler size on the properties of poly(lactic acid) (PLA)/graphene nanoplatelet (GNP) nanocomposites. Eur Polym J 2017;86:117–31. doi:https://doi.org/10.1016/j.eurpolymj.2016.10.045.

[18] Park JS, Yu L, Lee CS, Shin K, Han JH. Liquid-phase exfoliation of expanded graphites into graphene nanoplatelets using amphiphilic organic molecules. J Colloid Interface Sci 2014;417:379–84. doi:https://doi.org/10.1016/j.jcis.2013.11.066.

[19] Liu H, Gao J, Huang W, Dai K, Zheng G, Liu C, et al. Electrically conductive strain sensing polyurethane nanocomposites with synergistic carbon nanotubes and graphene bifillers. Nanoscale 2016;8:12977–89. doi:10.1039/c6nr02216b.

[20] Zhou G, Yao H, Zhou Y, Wang W, Peng M. Self-assembled complexes of graphene oxide and oxidized vapor-grown carbon fibers for simultaneously enhancing the strength and toughness of epoxy and multi-scale carbon fiber/epoxy composites. Carbon N Y 2018;137:6–18. doi:https://doi.org/10.1016/j.carbon.2018.05.014.

[21] Ma L, Wang G, Dai J. Preparation of a functional reduced graphene oxide and carbon nanotube hybrid and its reinforcement effects on the properties of polyimide composites. J Appl Polym Sci n.d.;134. doi:10.1002/app.44575.

[22] Bagotia N, Choudhary V, Sharma DK. Synergistic effect of graphene/multiwalled carbon nanotube hybrid fillers on mechanical, electrical and EMI shielding properties of polycarbonate/ethylene methyl acrylate nanocomposites. Compos Part B Eng 2019;159:378–88. doi:https://doi.org/10.1016/j.compositesb.2018.10.009.

[23] Cho B-G, Lee S, Hwang S-H, Han JH, Chae HG, Park Y-B. Influence of hybrid graphene oxide-carbon nanotube as a nano-filler on the interfacial interaction in nylon composites prepared by in situ interfacial polymerization. Carbon N Y 2018;140:324–37. doi:https://doi.org/10.1016/j.carbon.2018.08.041.

[24] Cao M, Du C, Guo H, Li X, Song S, Tezel FH, et al. Paving thermally conductive highway by 3D interconnected framework of carbon nanotube and graphene oxide in poly(vinylidene fluoride). Compos Part A Appl Sci Manuf 2018;115:331–40. doi:https://doi.org/10.1016/j.compositesa.2018.09.024.

[25] Wang E, Dong Y, Islam MDZ, Yu L, Liu F, Chen S, et al. Effect of graphene oxide-carbon nanotube hybrid filler on the mechanical property and thermal response speed of shape memory epoxy composites. Compos Sci Technol 2019;169:209–16. doi:https://doi.org/10.1016/j.compscitech.2018.11.022.

[26] Pinto VC, Ramos T, Alves ASF, Xavier J, Tavares PJ, Moreira PMGP, et al. Dispersion and failure analysis of PLA, PLA/GNP and PLA/CNT-COOH biodegradable nanocomposites by SEM and DIC inspection. Eng Fail Anal 2017;71:63–71. doi:https://doi.org/10.1016/j.engfailanal.2016.06.009.

[27] Jiang Z, Zhang H, Han J, Liu Z, Liu Y, Tang L. Percolation model of reinforcement efficiency for carbon nanotubes dispersed in thermoplastics. Compos Part A Appl Sci Manuf 2016;86:49–56. doi:https://doi.org/10.1016/j.compositesa.2016.03.031.

[28] Zare Y. Development of Halpin-Tsai model for polymer nanocomposites assuming interphase properties and nanofiller size. Polym Test 2016;51:69–73. doi:https://doi.org/10.1016/j.polymertesting.2016.02.010.

[29] Pontefisso A, Mishnaevsky L. Nanomorphology of graphene and CNT reinforced polymer and its effect on damage: Micromechanical numerical study. Compos Part B Eng 2016;96:338–49. doi:10.1016/j.compositesb.2016.04.006.

[30] Scaffaro R, Maio A. Optimization of two-step techniques engineered for the preparation of polyamide 6 graphene oxide nanocomposites. Compos Part B Eng 2019;165:55–64. doi:10.1016/j.compositesb.2018.11.107.

[31] Liu S, Sun H, Ning N, Zhang L, Tian M, Zhu W, et al. Aligned carbon nanotubes stabilized liquid phase exfoliated graphene hybrid and their polyurethane dielectric elastomers. Compos Sci Technol 2016;125:30–7. doi:10.1016/j.compscitech.2016.01.022.

[32] Scaffaro R, Botta L, Maio A, Gallo G. PLA graphene nanoplatelets nanocomposites: Physical properties and release kinetics of an antimicrobial agent. Compos Part B Eng 2017;109:139–46. doi:http://dx.doi.org/10.1016/j.compositesb.2016.10.058.

[33] Scaffaro R, Maio A, Botta L, Gulino EF, Gulli D. Tunable release of Chlorhexidine from Polycaprolactone-based filaments containing graphene nanoplatelets. Eur Polym J 2019;110:221–32. doi:10.1016/j.eurpolymj.2018.11.031.

[34] Dementev N, Osswald S, Gogotsi Y, Borguet E. Purification of carbon nanotubes by dynamic oxidation in air. J Mater Chem 2009;19:7904–8. doi:10.1039/B910217E.

[35] Feng Y, Zhang H, Hou Y, McNicholas TP, Yuan D, Yang S, et al. Room temperature purification of few-walled carbon nanotubes with high yield. ACS Nano 2008;2:1634–8. doi:10.1021/nn800388g.

[36] Scaffaro R, Maio A, Agnello S, Glisenti A. Plasma Functionalization of Multiwalled Carbon Nanotubes and Their Use in the Preparation of Nylon 6-Based Nanohybrids. Plasma Process Polym 2012;9:503–12. doi:10.1002/ppap.201100140.

[37] Scaffaro R, Maio A. Enhancing the mechanical performance of polymer based nanocomposites by plasma-modification of nanoparticles. Polym Test 2012;31:889–94. doi:10.1016/j.polymertesting.2012.06.006.

[38] Scaffaro R, Maio A, Re G Lo, Parisi A, Busacca A. Advanced piezoresistive sensor achieved by amphiphilic nanointerfaces of graphene oxide and biodegradable polymer blends. Compos Sci Technol 2018;156:166–76. doi:https://doi.org/10.1016/j.compscitech.2018.01.008.

[39] Maio A, Scaffaro R, Lentini L, Palumbo Piccionello A, Pibiri I. Perfluorocarbons–graphene oxide nanoplatforms as biocompatible oxygen reservoirs. Chem Eng J 2018;334:54–65. doi:10.1016/j.cej.2017.10.032.

[40] Maio A, Giallombardo D, Scaffaro R, Palumbo Piccionello A, Pibiri I. Synthesis of a fluorinated graphene oxide--silica nanohybrid: improving oxygen affinity. RSC Adv 2016;6:46037–47. doi:10.1039/c6ra02585d.

[41] Maio A, Agnello S, Khatibi R, Botta L, Alessi A, Piazza A, et al. A rapid and eco-friendly route to synthesize graphene-doped silica nanohybrids. J Alloys Compd 2016;664. doi:10.1016/j.jallcom.2015.12.137.

[42] Agnello S, Alessi A, Buscarino G, Piazza A, Maio A, Botta L, et al. Structural and thermal stability of graphene oxide-silica nanoparticles nanocomposites. J Alloys Compd 2017;695. doi:10.1016/j.jallcom.2016.11.044.

[43] Scaffaro R, Maio A, Lopresti F, Giallombardo D, Botta L, Bondì ML, et al. Synthesis and self-assembly of a PEGylated-graphene aerogel. Compos Sci Technol 2016;128:193–200. doi:10.1016/j.compscitech.2016.03.030.

[44] Botta L, Scaffaro R, Sutera F, Mistretta MC. Reprocessing of PLA/graphene nanoplatelets nanocomposites. Polymers (Basel) 2018;10. doi:10.3390/polym10010018.

[45] Sandhya PK, Sreekala MS, Padmanabhan M, Jesitha K, Thomas S. Effect of starch reduced graphene oxide on thermal and mechanical properties of phenol formaldehyde resin nanocomposites. Compos Part B Eng 2019;167:83–92. doi:https://doi.org/10.1016/j.compositesb.2018.12.009.

[46] Halpin JC. Stiffness and Expansion Estimates for Oriented Short Fiber Composites. J Compos Mater 1969;3:732–4. doi:10.1177/002199836900300419.

[47] Scaffaro R, Maio A, Gulino EF, Megna B. Structure-property relationship of PLA-Opuntia Ficus Indica biocomposites. Compos Part B Eng 2019;167:199–206. doi:https://doi.org/10.1016/j.compositesb.2018.12.025.

[48] Hu J, Dong S, Wu B, Zhang X, Zhou H, Wang Z, et al. Tailoring Carbon Fiber/Carbon Nanotubes Interface to Optimize Mechanical Properties of Cf-CNTs/SiC Composites. Int J Appl Ceram Technol 2014;11:207–17. doi:10.1111/ijac.12100.

[49] Wang W, Yokoyama A, Liao S, Omori M, Zhu Y, Uo M, et al. Preparation and characteristics of a binderless carbon nanotube monolith and its biocompatibility. Mater Sci Eng C 2008;28:1082–6. doi:https://doi.org/10.1016/j.msec.2007.04.038.

[50] Scaffaro R, Maio A, Lopresti F, Botta L. Nanocarbons in electrospun polymeric nanomats for tissue engineering: A review. Polymers (Basel) 2017;9. doi:10.3390/polym9020076.

[51] Scaffaro R, Maio A. A green method to prepare nanosilica modified graphene oxide to inhibit nanoparticles re-aggregation during melt processing. Chem Eng J 2017;308:1034–47. doi:http://dx.doi.org/10.1016/j.cej.2016.09.131.

[52] Maio A, Fucarino R, Khatibi R, Rosselli S, Bruno M, Scaffaro R. A novel approach to prevent graphene oxide re-aggregation during the melt compounding with polymers. Compos Sci Technol 2015;119:131–7. doi:http://dx.doi.org/10.1016/j.compscitech.2015.10.006.

[53] Gong S, Cui W, Zhang Q, Cao A, Jiang L, Cheng Q. Integrated Ternary Bioinspired Nanocomposites via Synergistic Toughening of Reduced Graphene Oxide and Double-Walled Carbon Nanotubes. ACS Nano 2015;9:11568–73. doi:10.1021/acsnano.5b05252.

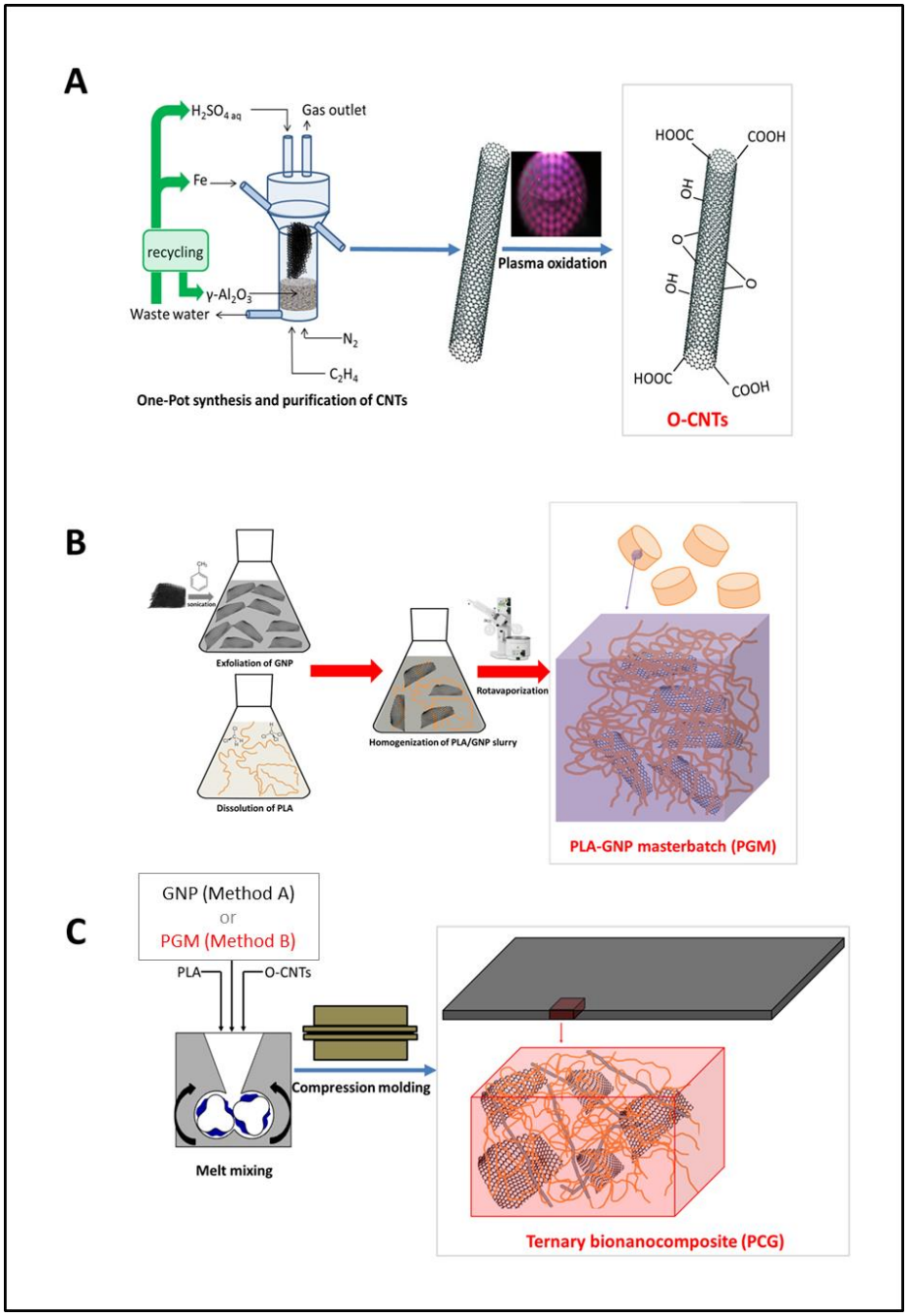

Fig. 1. Route followed to prepare ternary bionanocomposites

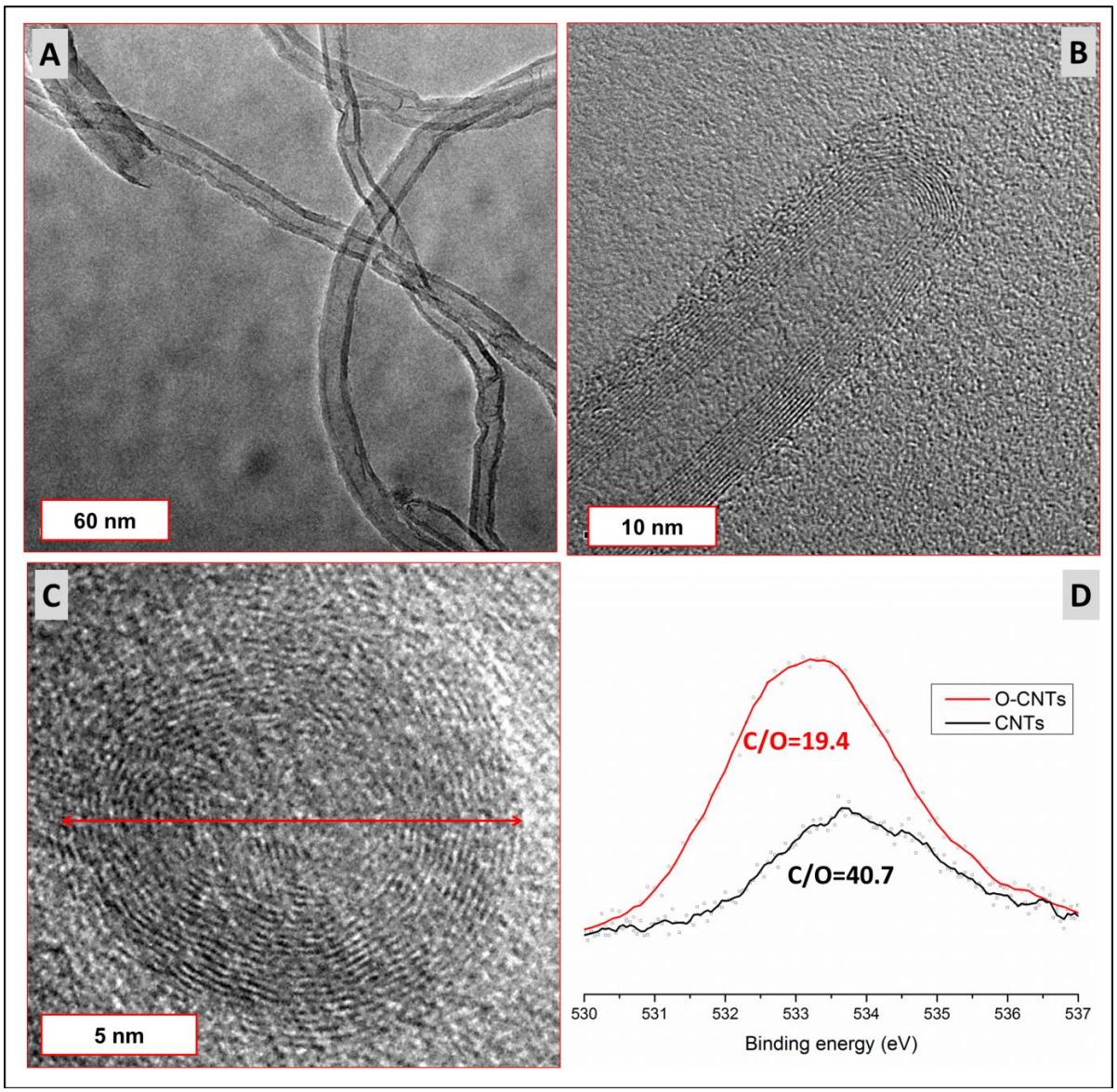

Fig. 2. A) TEM micrograph of O-CNTs highlighting the defects imparted by plasma-treatment; B-C) detailed TEM analysis of sidewalls and tip of individually dispersed O-CNTs; D) O1s XPS (and C/O ratio calculated by elemental analysis) before and after plasma treatment.

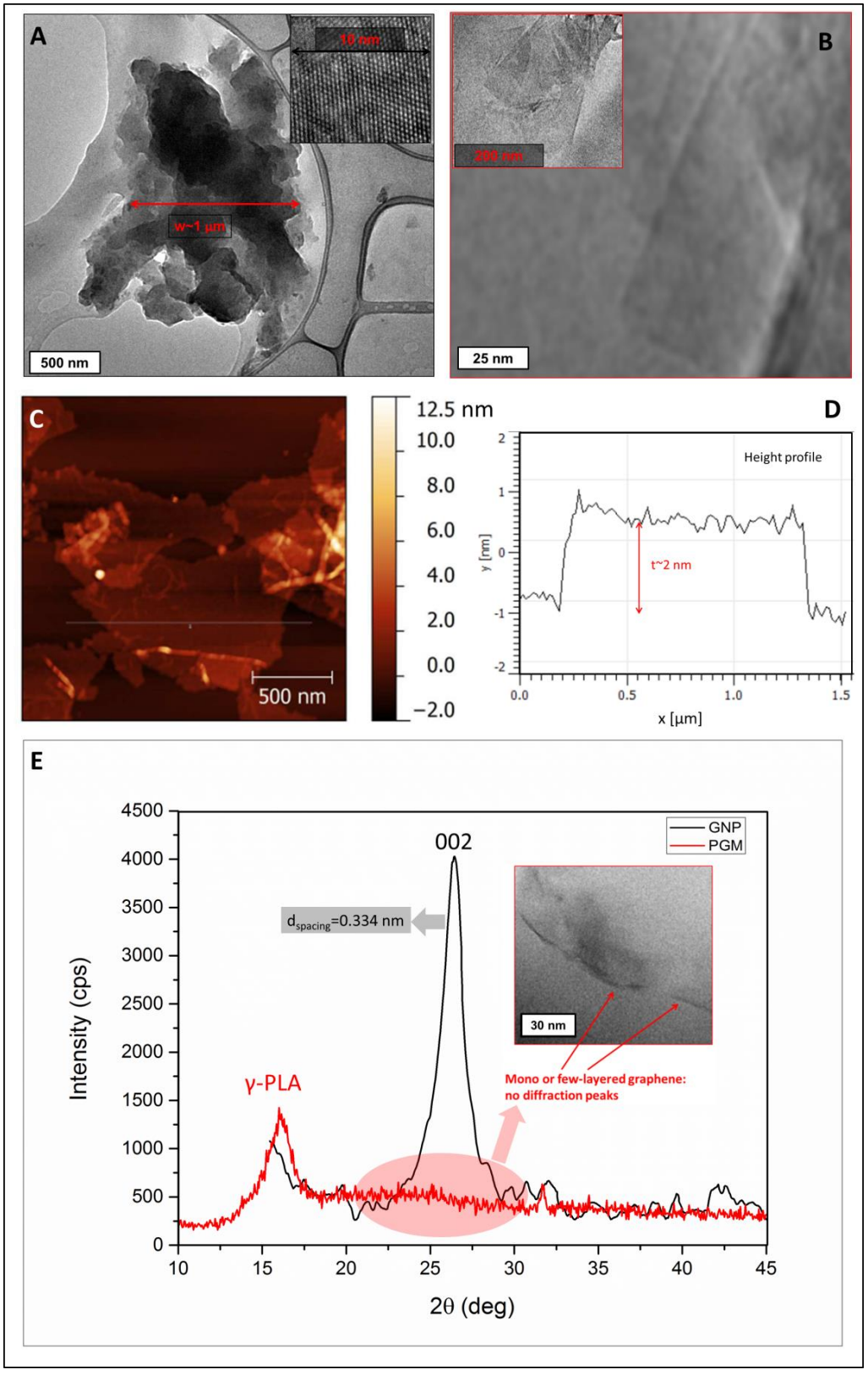

Fig. 3. Characterization of GNP and PGM: A) TEM micrograph of GNP submicrometric aggregates (inset: graphenic nanopattern); B) exfoliated GNP into mono or few-layered lamellae in PGM; C-D) AFM analysis together with height profile; E) XRD patterns of GNP and PGM to further confirm the exfoliation of GNP into few-layered graphene sheets.

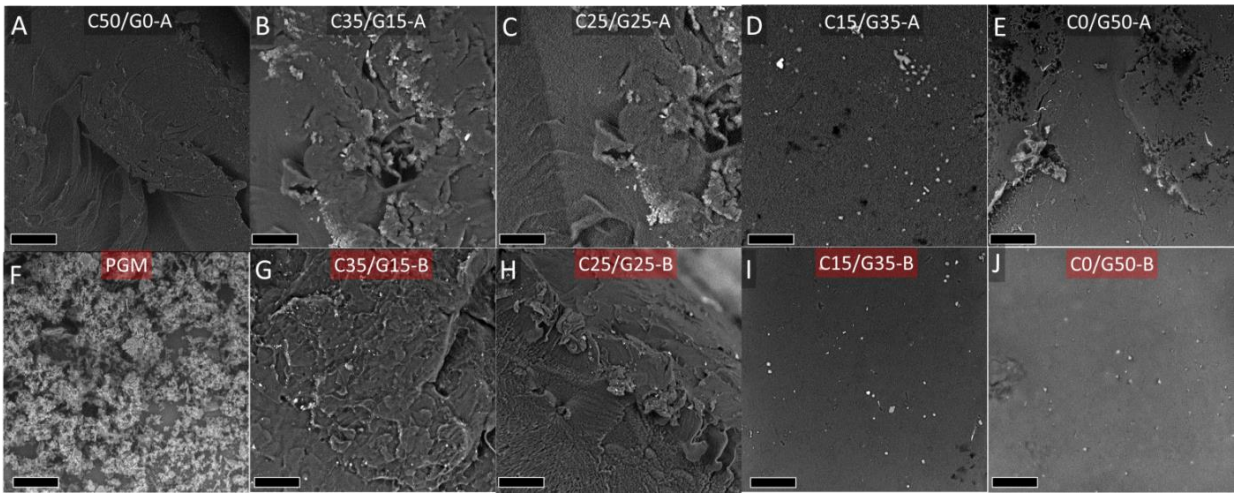

Fig. 4. SEM analysis of nanocomposites at low resolution to detect aggregates (scale bar=100 μm)

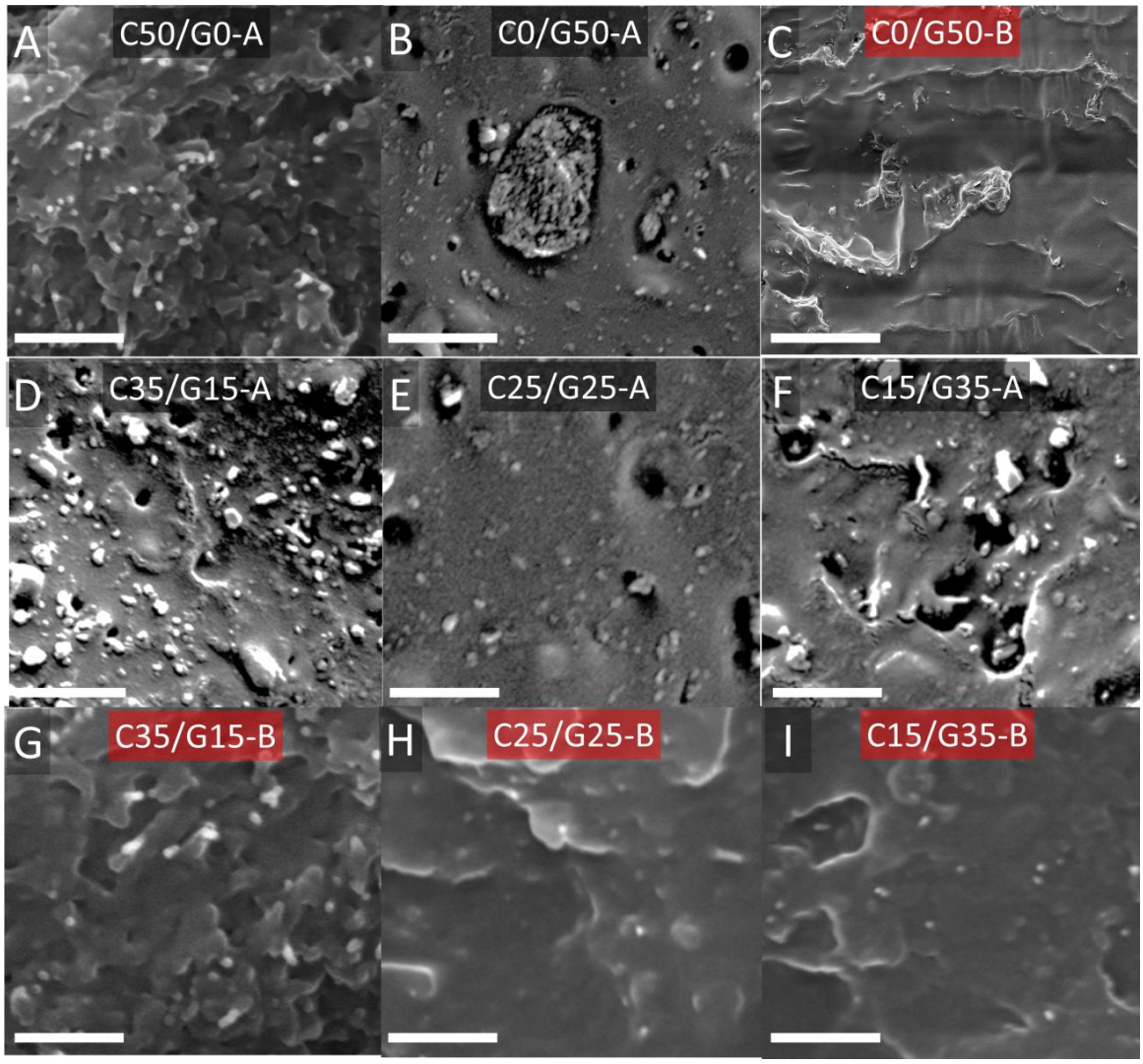

Fig. 5. Detailed SEM micrographs of nanocomposites prepared. Scale bar=5 μm

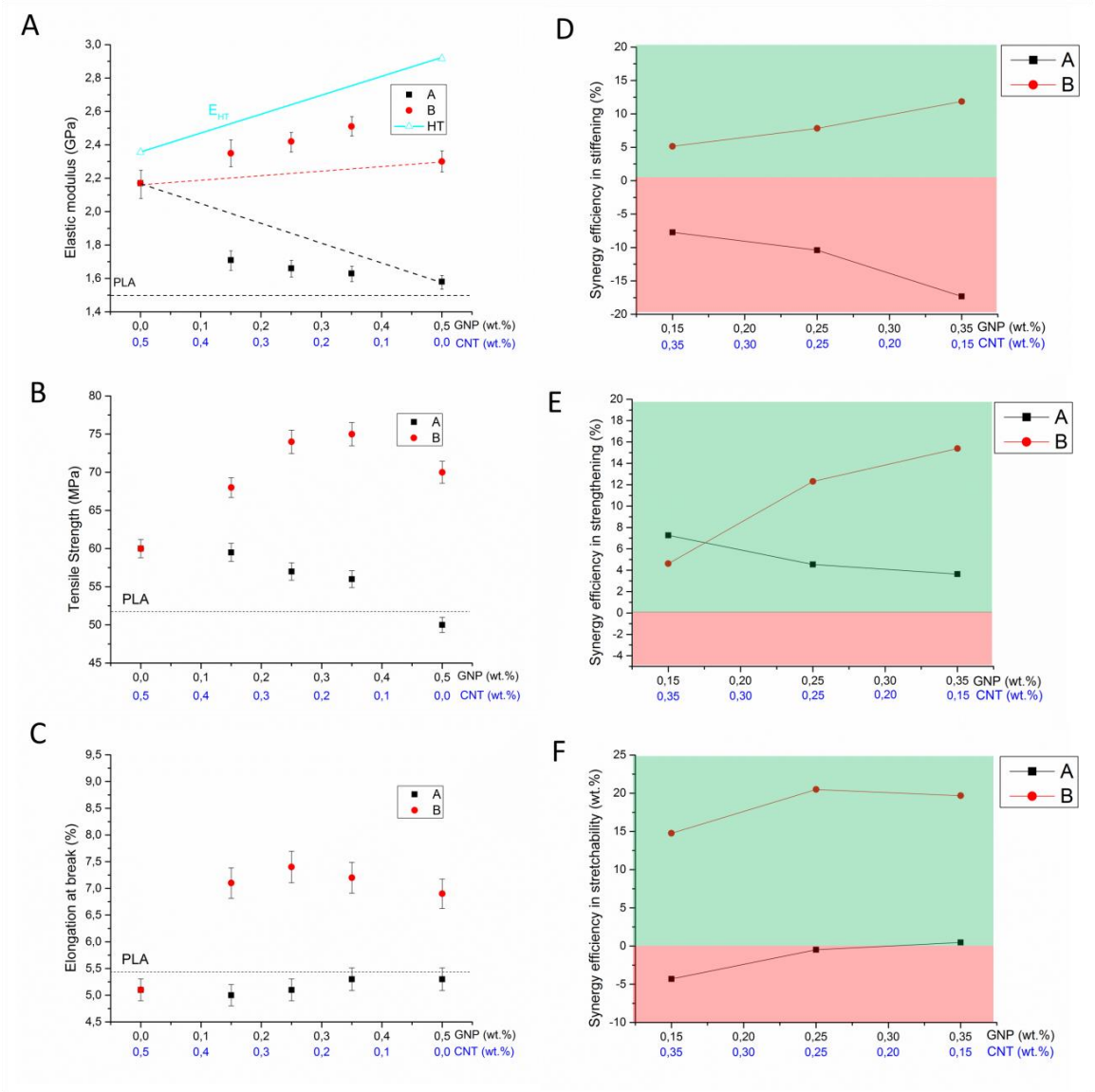

Fig. 6. Elastic modulus (A), tensile strength (B), elongation at break (C) together with synergetic efficiency in stiffening (D), strengthening (E) and stretchability (F) as a function of CNT and graphene content.

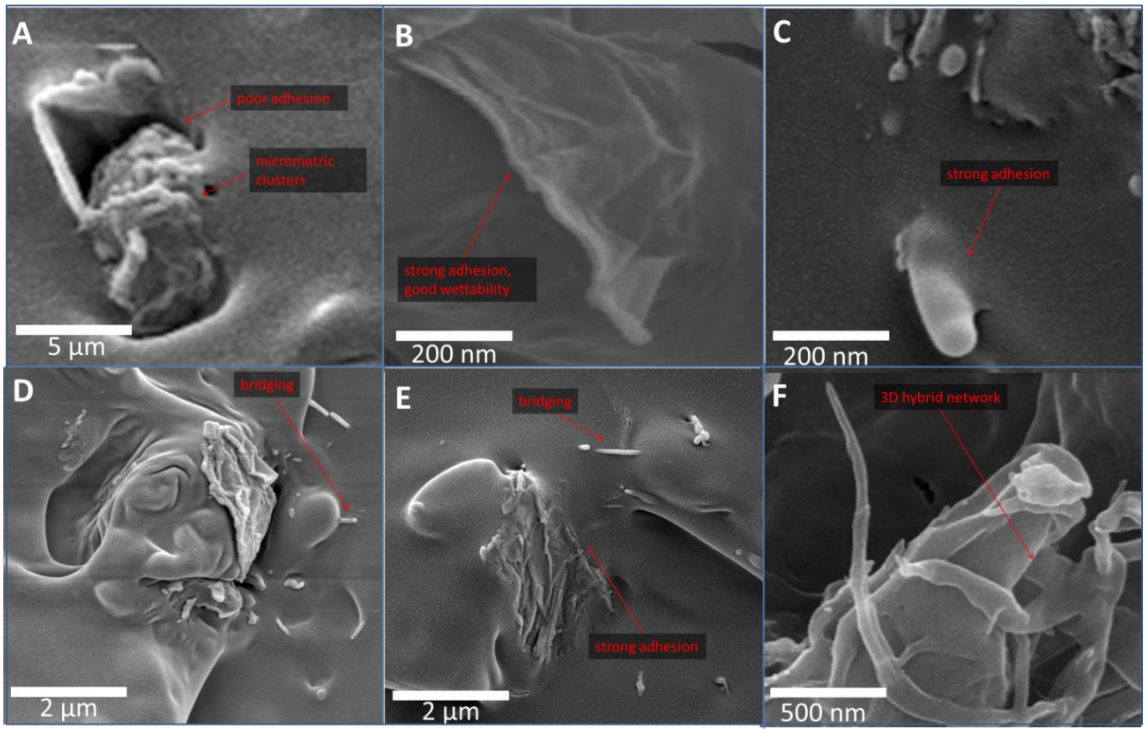

Fig. 7. Detailed SEM micrographs at various magnitudes describing interphase of C0/G50-A (A), C0/G50-B (B), C50/G0-A (C), C35/G15-B (D), C25/G25-B (E) and C15/G35-B (F).